19th Australasian Fluid Mechanics Conference
Melbourne, Australia
8–11 December 2014

# Flow Structures on a Low-Aspect-Ratio Wing Undergoing a Pitch-Ramp–Hold Manoeuvre in a Uniform Cross-Flow

**A. Agon, M. Giacobello and J. L. Palmer**

Defence Science and Technology Organisation

Fishermans Bend, Victoria 3207, Australia

## Abstract

A computational fluid dynamics (CFD) study has been conducted to investigate the development of the vortical flow structure on a thin, rectangular wing undergoing a pitch-ramp–hold manoeuvre in a steady on-coming flow. The motion represents a simplification of the flapping-wing motion of insects and serves as a canonical test case to provide insight into the unsteady aerodynamics of flapping-wing flight, as well as CFD-modelling heuristics. A freestream Reynolds number based on wing chord of $10^3$ was considered, and the wing, which had an aspect ratio of four, was rotated about its leading edge from an angle of attack of zero to 45°. The study explored the effects of the pitch-ramping rate and the smoothness of the transitions between the piecewise components of the pitch-ramp–hold manoeuvre.

The pitching motion generates a highly unsteady, three-dimensional flow structure in the wing wake. Varying the motion parameters has a distinct effect on the aerodynamic loading, with increased pitching rate and reduced smoothing of the pitch-ramp–hold manoeuvre leading to higher aerodynamic loads. However, above a critical level, a reduction of the smoothing results in little increase in the instantaneous aerodynamic loading. The maximum lift and drag coefficients were found to correlate with the pitch-ramping rate, with motion at the highest rate simulated yielding the highest aerodynamic loading.

## Introduction

Flapping-wing flight is attracting growing interest due to its potential application in 'micro' air vehicles (MAVs). To understand the fundamental mechanisms of flapping-wing aerodynamics at low-to-moderate Reynolds numbers, various canonical cases have been proposed [6]. They comprise of a sinusoidal increase in the pitch angle of a wing (simplified to a flat plate) with time. However, to avoid function spikes due to discontinuities in the pitching rate, a smoothing function used by Eldredge *et al.* [2] and Garmann *et al.* [3] was adopted:

$$\theta(\tau) = \frac{\theta_0}{2a\Delta\tau}\ln\left[\frac{\cosh\left(a(\tau-\tau_1)\right)}{\cosh\left(a(\tau-\tau_2)\right)}\right] + \frac{1}{2}\theta_0, \qquad (1)$$

where $\theta$ is the pitch angle (angle of attack), $\theta_0$ is the maximum pitch angle in the manoeuvre, and $a$ is a parameter that controls the 'smoothness' of the transitions. Time, $t$, is non-dimensionalised by the convective timescale:

$$\tau = tU/c, \qquad (2)$$

where $U$ is the freestream velocity and $c$ is the chord length. The time that would be taken for a linear pitch-ramping manoeuvre (without smoothing) is $\Delta\tau = \tau_2 - \tau_1$, where $\tau_1$ and $\tau_2$ are the times at which the motion would start and stop, respectively.

The motion described by Equation (1) for a case in which the pitch-ramping manoeuvre occurs in the time taken for the flow to travel one chord length ($\Delta\tau = 1$, with $\tau_1 = 0.5$ and $\tau_2 = 1.5$) is shown in Figure 1 for two values of the smoothing parameter, $a = 5$ and 11. The variation of the smoothing parameter affects both the pitch-angle history and the pitching rate ($\theta'$).

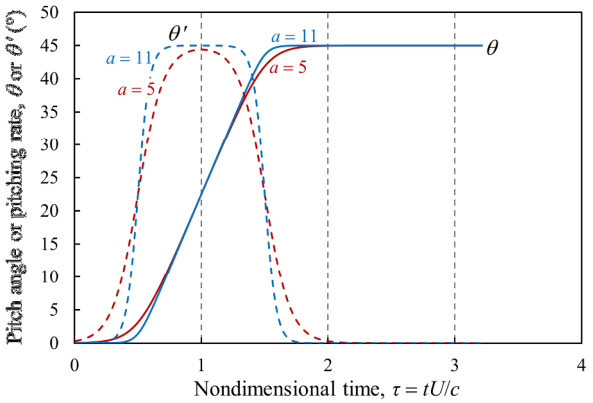


Figure 1. Smoothed pitch-ramping motion described by Equation (1) with $\Delta\tau = 1$, $\tau_1 = 0.5$, $\tau_2 = 1.5$, and $a = 5$ or 11.

In this study, flow conditions at a Reynolds number ($Re$) of $10^3$ were investigated (where $Re = Uc/\nu$ and $\nu$ is the kinematic viscosity of the fluid). A parameterisation study was conducted to determine the sensitivity of the aerodynamic forces and three-dimensional flow structure to the pitching rate and the details of the motion (its smoothing). The motion described by Equation (1) was used, and pitch-ramping timescales of $\Delta\tau$ = [1, 2, 3] were tested for a fixed value of the smoothing parameter ($a = 5$) to assess the effect of pitching rate. To evaluate the influence of the smoothing parameter, values of $a$ = [0.5, 1, 3, 5, 11] were considered for a fixed value of the pitch-ramping rate ($\Delta\tau = 2$).

## Computational Setup

### Numerical Procedure

Due to the moderate Reynolds number considered, the Navier–Stokes equations were solved directly using the ANSYS Fluent pressure-based incompressible solver [1]. Second-order spatial and temporal discretisation with upwind differencing was used for all simulations and pressure–velocity coupling was achieved with the SIMPLEC scheme.

The grid comprised a prismatic inflation layer that extended from the wing surface to beyond the steady-state, laminar boundary layer (at $\theta = 0$). Beyond that, the unstructured tetrahedral mesh extended to the farfield boundary. A grid with a higher density was used immediately aft of the wing to resolve the wake. The computational domain was spherical and extended forty chord lengths in all directions. A domain of this size has been found to be sufficient to capture the flow structure in prior computational studies of similar problems [5]. Prior findings [6, 3] also indicate

that changes in Reynolds number in the range of $10^3$ to $4\times10^4$ minimally affect the temporal evolution of similar flowfields.

### Wing Geometry and Pitching Motion

The wing under consideration has a chord of $c$ and a span of $4c$, yielding an aspect ratio of 4. Its thickness is equal to 5% of the chord. The leading and trailing edges of the wing are rounded to conform to the benchmark cases [6]. The meshing procedure is also simplified by rounding the sides of the wing.

The pitching motion occurs about the leading edge of the wing, and the pitch angle ramps from $\theta = 0$ to 45°, as shown in Figure 1. In the Fluent simulation, the wing motion is prescribed via a user-defined function and applied as a mesh motion. Initially a simulation with the wing at $\theta = 0$ was run, and this formed the starting point for each transient simulation.

### Effect of Spatial and Temporal Resolution

A temporal-sensitivity study was performed to verify the numerical accuracy of the CFD technique, with time steps varying from $\Delta t = 2.5\times10^{-5}$ s to $2\times10^{-4}$ s (with a doubling in each successive simulation) for the fastest pitching manoeuvre [defined by Equation (1) with $\Delta\tau = 1$ and $a = 11$]. The results show that the temporal resolution predominantly affects the peaks and troughs of the aerodynamic loads. This is illustrated in Figure 3(a), which shows the lift coefficient, $C_L$ [where $C_L = L/(\frac{1}{2}\rho U^2)$, $L$ is the lift force, and $\rho$ is the density of the fluid]. Refining the time-step from $\Delta t = 5\times10^{-5}$ s to $2.5\times10^{-5}$ s resulted in only slight changes in the computed force histories (< 1% in the lift and drag forces); thus a time step of $5\times10^{-5}$ s was chosen for all simulations presented herein.

A spatial-sensitivity study was also performed to ensure that the CFD results were independent of mesh size. The fastest pitching manoeuvre was again chosen; and three grid resolutions were compared: a coarse grid of ~6 million elements, a medium-density grid of ~10 million elements, and a fine grid of ~24 million elements. Figure 3(b) shows the lift and drag coefficients computed using the different grids [where the drag coefficient is given by $C_D = D/(\frac{1}{2}\rho U^2)$ and $D$ is the drag force]. These results indicate that there is a negligible difference in the lift and drag forces on the wing computed using the different grids. Similarly, only minor differences were observed in the vortical wake structure. The finest grid was chosen for the remainder of the study to ensure that small-scale wake structures were resolved.

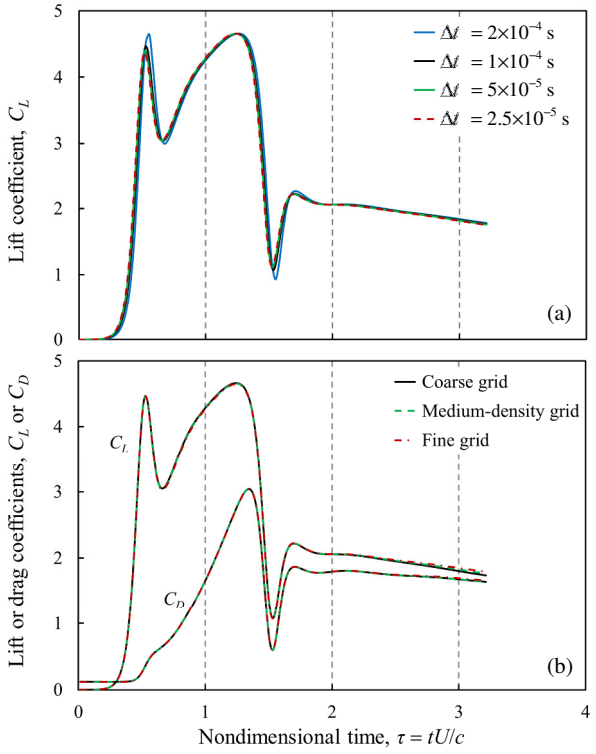


Figure 3. (a) Lift-coefficient histories from simulations with different time steps; and (b) lift- and drag-coefficient histories from simulations with different grid resolutions. In each case, the motion of the wing is described by Equation (1) with $\Delta\tau = 1$ and $a = 11$.

## Results

### Effect of Motion Parameters on Flow Structure

The second invariant of the velocity-gradient tensor, $Q$ is used to aid in vortical-flow visualisation. The $Q$ criterion is defined by

$$Q = \tfrac{1}{2}\left(\Omega_{ij}^2 - S_{ij}^2\right), \qquad (3)$$

where $\Omega_{ij}$ is a measure of the strength of the local vorticity and $S_{ij}$ is a measure of the irrotational stretching [4]. The construction of iso-surfaces of constant $Q$ (> 0) enables the visualisation of rotational flow structures.

#### *Pitch-Ramping Rate*

To establish the effect of the pitch-ramping rate, the flows generated by wing motions with $\Delta\tau = 1$ and $\Delta\tau = 3$ at a fixed value of the smoothing parameter, $a = 5$, were examined. The resulting

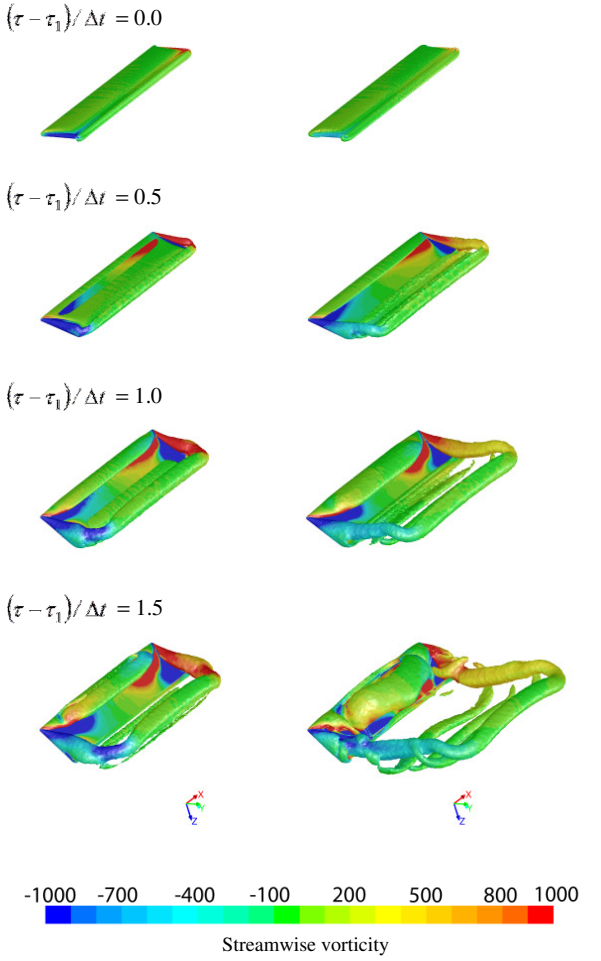


Figure 2. Instantaneous iso-surfaces of $Q = 10^4$ s$^{-2}$, coloured by streamwise vorticity. The wing motion is described by Equation (1) with $a = 5$ and $\Delta\tau = 1$ (left panel) and $\Delta\tau = 3$ (right panel), and snapshots of various moments in the wing motion are displayed.

flow structures are shown at various instants of time during the development of the flowfield in Figure 2. For the times at which the flow is shown, the vortical structure remains symmetric about the wing's centreline. For both $\Delta\tau = 1$ and $\Delta\tau = 3$, a leading-edge vortex (LEV) is formed and remains attached to the wing, whereas a 'starting' trailing-edge vortex (TEV) of opposite sign detaches from the wing surface. The TEV remains bound to the wing and forms a contra-rotating trailing vortex pair (as evident from the equal and opposite magnitudes of the streamwise-vorticity contours). Owing to the longer convective time over which the wing undergoes the pitching manoeuvre for the case with $\Delta\tau = 3$, the LEV separates from the wing near the centreline, forming a vortex loop; while a regular series of TEVs, subsequent to the primary starting TEV, are shed.

### *Motion-Smoothing Parameter*

Figure 4 shows the temporal evolution of the flowfield obtained from simulations with $\Delta\tau = 2$ and values of smoothing parameter, $a$ = 1, 5, and 11 (left-to-right). A contra-rotating TEV pair is evident in all cases up to $\tau \approx 18$. At later times, the wake is characterised by asymmetrical shedding of large-scale vortex loops and a loss of symmetry about the wing centreline, highlighting the need for a fully three-dimensional solution.

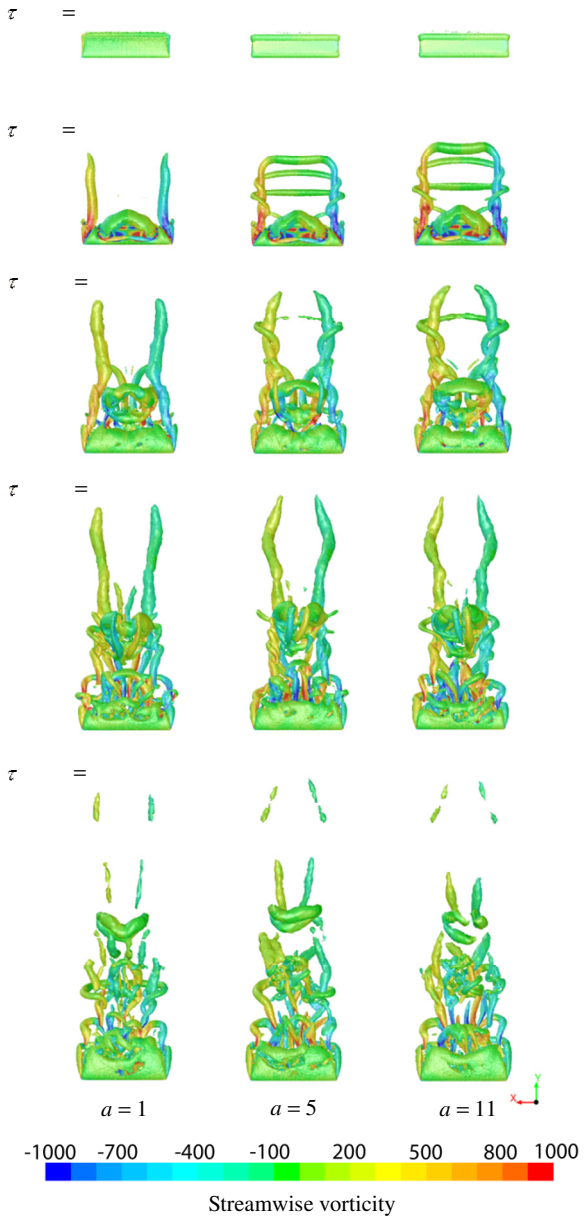


Figure 4. Iso-surfaces of $Q = 10^4\ s^{-2}$, coloured by streamwise vorticity and showing the temporal evolution of the flow for $\Delta\tau = 2$ and values of $a$ = 1, 5, and 11 (left-to-right). Note that $\tau_1 = 5$ and $\tau_2 = 7$.

Early in the pitching manoeuvre ($4.4 < \tau < 13.2$) the flowfields generated with different amounts of motion smoothing show distinct differences. The three vortex loops apparent in the cases with $a$ = 5 and 11 are not present in the flowfield computed with the greatest amount of smoothing ($a$ = 1).

## Effect of Motion Parameters on Aerodynamic Loading

Figure 5 shows the evolution of the lift and drag forces computed for wing motions with $\Delta\tau = 1$ and differing amounts of smoothing (different values of $a$). The case with least smoothing ($a$ = 11) shows behaviour unlike the cases with smoother transitions in the pitch-ramp–hold manoeuvre. In particular, local maxima and minima in $C_L$ are encountered prior to and after the peak in lift, as seen in Figure 5(a). Similar features are seen in the drag force, as shown in Figure 5(b), though the initial deviation is significantly smaller than that seen in the lift force.

Figure 6 shows the effect of the smoothing parameter for cases with $\Delta\tau = 2$. The peaks at $\tau \approx 6$ and 13 correspond to the shedding of two leading-edge vortices. The frequency at which they are shed is not be a strong function of $a$, although the first peak in both lift and drag is strongly coupled with $a$. The peak at $\tau \approx 13$ is unaffected by the value of $a$. The maximum aerodynamic loads associated with the pitch-ramping of the wing are plotted in Figure 7 to establish the relationship between the smoothing parameter ($a$) and the peak lift and drag coefficients ($C_{L,\max}$ and $C_{D,\max}$, respectively). The data indicates that for the range of $\Delta\tau$ tested, values of $a$ in excess of 5 result in only small changes to the maximum loading.

The case with the fastest pitch-ramping rate ($\Delta\tau = 1$) consist-

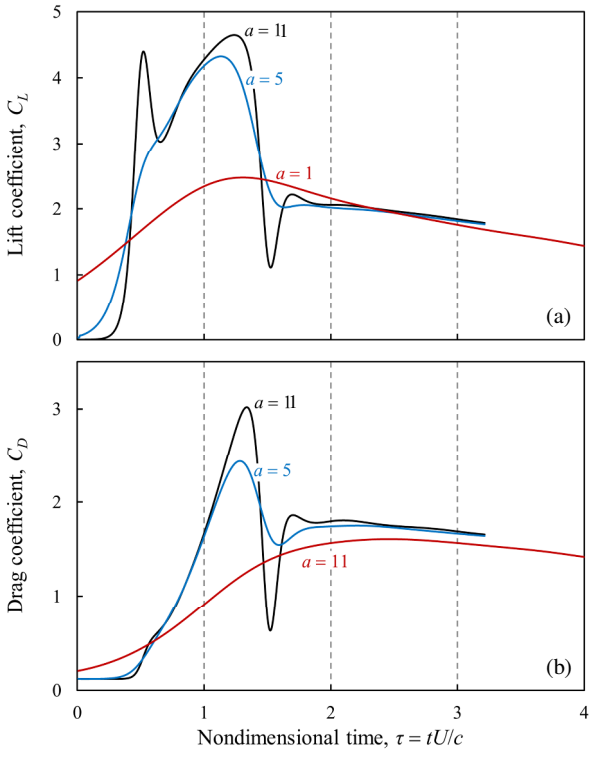


Figure 5. Effect of motion-smoothing parameter, $a$, on (a) lift and (b) drag coefficient for wing motion with $\Delta\tau = 1$ and $\tau_1 = 0.5$.

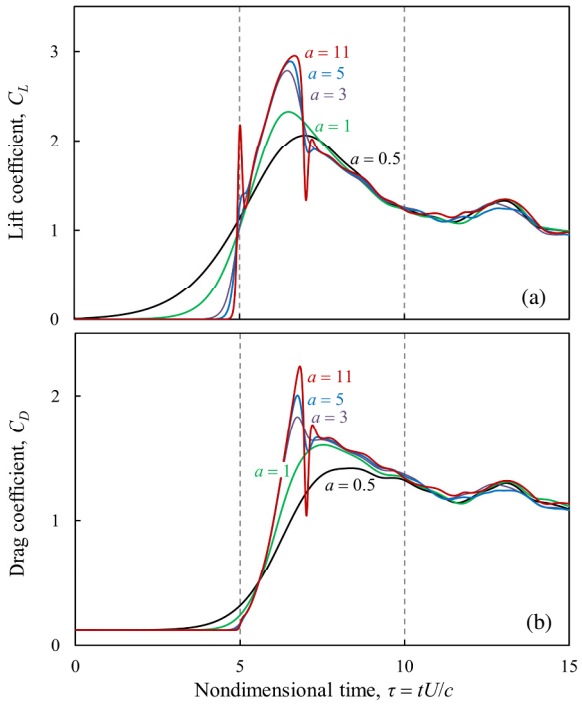


Figure 6. Effect of smoothing parameter, $a$, on (a) lift and (b) drag coefficient for wing motion with $\Delta\tau = 2$ and $\tau_1 = 5$.

ently generates larger loadings than do the slower motions; and the loading increases with the smoothing parameter ($a$). A drop in aerodynamic loading is seen with an increase in $\Delta\tau$, indicating that faster, more abrupt motions (decreases in $\Delta\tau$ and increases in $a$, respectively) cause higher lift and drag.

To investigate whether the pitch angle or pitching rate has a larger effect on the aerodynamic loads, Figure 8 presents the lift coefficient versus the pitch angle for wing motions with $\Delta\tau = 2$ and various amounts of smoothing. The maximum lift is seen to occur at pitch angles of 30° and 40°, as the motion begins to decelerate (Fig. 1), rather than at the maximum pitch angle.

## Conclusion

A pitch-ramp–hold manoeuvre with a flat, rectangular wing in a steady on-coming flow has been investigated by direct numerical simulation, and the aerodynamic loading coefficients and temporal evolution of the flow structure have been examined. Flow visualisation using the $Q$-criterion revealed a complex, highly vortical flow characterised by a leading-edge vortex that remains

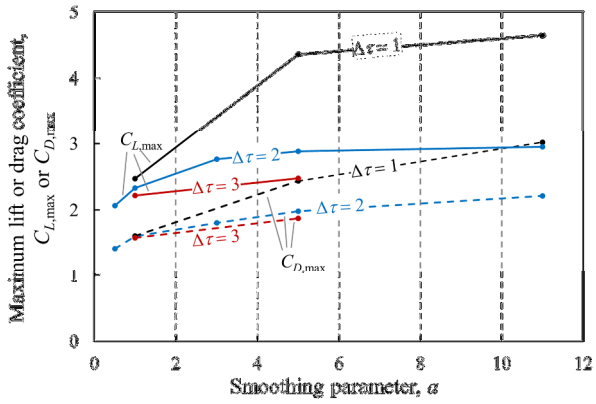


Figure 7. Effect of motion-smoothing parameter, $a$, on $C_{L,\max}$ and $C_{D,\max}$ for wing motions with $\Delta\tau = 1$, 2, and 3.

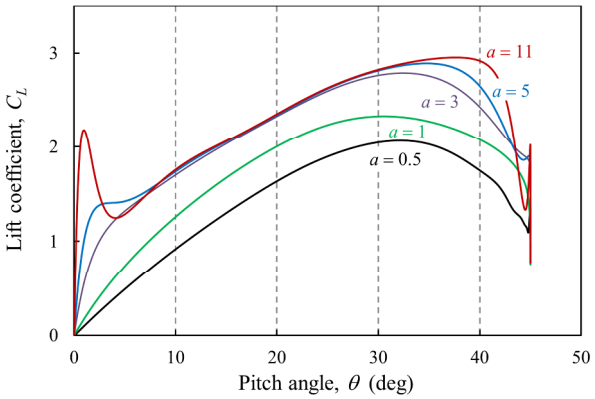


Figure 8. Aerodynamic loading as a function of pitch angle for wing motions with $\Delta\tau = 2$ and various values of the smoothing parameter, $a$.

attached during pitch-ramping and a bound trailing-edge 'starting' vortex that detaches and is convected downstream. The motion parameters investigated were shown to strongly affect both loading parameters (lift and drag), as well as the flowfield.

The canonical problem studied here provides designers of flapping-wing 'micro' aircraft valuable insight into the relationship between their wing kinematics and their aerodynamics. The motion studied is similar to the pitch reversals at the extremes of each wing stroke executed by insects. The pitch-ramping rate of the wings has been shown to strongly influence the lift generated, with more rapid ramping yielding higher aerodynamic forces. Abrupt motion transitions have also been shown to produce higher lift and drag than smoother ones, up to a point at which the dependence of the peak lift on the degree of motion smoothing declines. The aircraft designer is presented with guidance on the rate of pitch reversal and the degree of motion smoothing. Such factors, along with structural and power considerations, will govern the wing kinematics of practical flapping-wing mechanisms.

## Acknowledgements

This project is supported by DSTO's Strategic Research Initiative on Autonomous Systems. The authors thank NATO STO AVT-202, led by Dr Michael Ol (US AFRL) and Prof Holger Babinsky (Cambridge University), for ideas that generated this research.

## References

[1] ANSYS, Inc., *ANSYS Fluent*, 2013. Available from: www.ansys.com.

[2] Eldredge, J.D., Wang, C., & Ol, M.V., A Computational Study of a Canonical Pitch-Up, Pitch-Down Wing Maneuver, in *39th AIAA Fluid Dyn. Conf.*, AIAA, 2009.

[3] Garmann, D.J., Visbal, M.R., & Orkwis, P.D., Three-Dimensional Flow Structure and Aerodynamic Loading on a Revolving Wing. *Phys. Fluids,* **25**, 2013.

[4] Hunt, J.C.R., Wray, A.A., & Moin, P., Eddies, Streams, and Convergence Zones in Turbulent Flows, in *Proceedings of the Summer Program*, Report CTR-S88, Stanford, Center for Turbulence Research, 1988, 193–208.

[5] Lian, Y., & Ol, M.V., Computation and Experiments on a Low Aspect Ratio Pitching Flat Plate, in *48th AIAA Aero. Sci. Meet.*, AIAA 2010-385, 2010.

[6] Ol, M.V., Altman, A., Eldredge, J.D., Garmann, D.J., & Lian, Y., Résumé of the AIAA FDTC Low Reynolds Number Discussion Group's Canonical Cases, in *48th AIAA Aero. Sci. Meet.*, AIAA 2010-1085, 2010.